FORMULATION AND CHARACTERIZATION OF THERMOSENSITIVE CHITOSAN HYDROGEL LOADED WITH ERLOTINIB: FULL FACTORIAL DESIGN OF RELEASE DATA

Arafat Abdelzaher[1], Ahmed M. Mohammed[2], and Shaaban K. Osman[2]*

[1]General Authority for Health Insurance, South Valley Branch, Egypt.

[2]Department of Pharmaceutics and Pharmaceutical Technology, Faculty of Pharmacy, Al-Azhar University, Assiut 71524, Egypt

*Corresponding author: E-mail: shaabanosman@azhar.edu.eg

ABSTRACT

Erlotinib is a Tyrosine Kinase Inhibitor (TKI) that is utilized in the treatment of various types of tumors expressing the epidermal growth factor receptors (EGFR) protein. However, it is characterized as a drug with poor solubility in water and a high affinity for blood plasma proteins. According to the biopharmaceutical classification system (BCS), Erlotinib falls under class two, where its solubility acts as the rate-limiting step for its bioavailability. In systemic administration, Erlotinib exhibits a bioavailability of approximately 60%, but it also presents several systemic side effects, which can be severe in certain cases due to its poor solubility in water and its strong binding to plasma proteins. To address the issue of low bioavailability, we pursued an efficient approach to enhance the solubility of Erlotinib. nanoparticle formation using the non-solvent method, and dynamic light scattering (DLS) and in vitro dissolution studies were employed to characterize the Erlotinib nanoparticles (ETB-NPs). These studies also produced favorable outcomes, demonstrating the successful improvement of Erlotinib's solubility through nanoparticle formation. Following the solubility enhancement, the drug was formulated into a local injectable hydrogel for targeted delivery. This formulation exhibited significant improvements in the release of Erlotinib. The solubility enhancement and localized administration of Erlotinib within the tumor microenvironment facilitated controlled release and contributed to the observed enhancements. The chitosan hydrogel used as the carrier system for Erlotinib was thoroughly characterized using various studies, including viscosity measurements, pH determination, and in vitro release studies, all of which yielded positive results.

Keywords: Erlotinib, cancer, tyrosine kinase, hydrogels, inclusion complex, in vitro release, Nanoparticles, Chitosan

1. Introduction

Erlotinib HCL (N-(3-ethynylphenyl)-6,7-bis(2-methoxyethoxy) quinazoline-4-amine) is a member of TKIs, specifically a quinazoline derivative that acts as an ATP competitor by binding to EGFR-TK. It was approved by the FDA in 2004 as a monotherapy for the treatment of advanced non-small cell lung cancer (NSCLC). In 2005, it received approval for the treatment of metastatic pancreatic carcinoma in combination with Gemcitabine, and in 2013, it was approved as a first-line treatment for NSCLC. (Pandey *et al.*, 2019;Uddin etal, 2020;Mandal *et al.*, 2016).

Although Erlotinib demonstrates good efficacy in combating cancer, it is associated with several side effects due to its poor solubility in water and its high affinity for binding with blood plasma proteins. According to the biopharmaceutical classification system, Erlotinib falls into category two, indicating limited bioavailability resulting from its poor aqueous solubility (S_0 = 12.46 μM), It has a high lipophilicity with a log P value of 2.75 and a protonation constant of log K=5.33.(Erdoğar *et al.*, 2021;Pandey *et al.*, 2019;Lee *et al.*, 2021;Salehi *et al.*, 2021;Honeywell *et al.*, 2020;Betriu et al., 2021). Various strategies have been employed to enhance the solubility of Erlotinib (ETB). These approaches can be categorized as physical or chemical methods and encompass techniques such as particle size reduction, crystal engineering, salt formation, solid dispersion, and complexation (Salehi et al., 2021). These approaches have been widely utilized to improve the solubility of poorly water-soluble drugs (Honeywell *et al.*, 2020;Betriu et al. , 2021;Pandey *et al.*, 2019;Zhang *et al.*, 2019).

Nanocrystals preparation is one of the newest physical strategies to improve the dissolution rate of poorly water-soluble materials(Mostafa et al. , 2022;Amin *et al.* , *et al.*, 2023). According to the Noyes- Whitney equation, the particle size reduction will result in an increased surface area to volume ratio which increases the solubility and dissolution rate of badly soluble drugs (Mostafa *et al.* , 2022). Improvement of the solubility of low soluble highly permeable molecules will subsequently enhance the bioavailability and efficacy of such drugs (Merisko-liversidge and Liversidge, 2008;Amin *et al.*, 2023;Wang *et al.*, 2018;Hassan *et al.*, 2022;Pandey *et al.*, 2019).

Nanocrystals can be prepared using either the top-down or bottom-up method (Betriu et al., 2021; Zhang *et al.*, 2019). In the top-down technique, larger particles are mechanically comminuted into smaller nanoparticles using a high-energy mill. This method requires a significant amount of energy input, consuming long time, and may introduce contamination. On the other hand, the bottom-up approach involves the precipitation of nanoparticles from dissolved drug molecules. This method yields better product output by achieving a homogeneous particle distribution with lower energy input. It also utilizes cost-effective equipment and occurs at ambient temperatures and atmospheric pressure, thereby preserving the stability of the processed materials (Betriu et al., 2021; Amin et al., 2023; L. Zhang et al., 2019; Hassan et al., 2022; Elkarim et al. , 2022). To ensure the production of stable nanoparticles, it is essential to coat the particle's surface with a suitable stabilizer. This coating serves multiple purposes, including preventing particle growth and aggregation during preparation and storage. Additionally, it contributes to the enhancement of solubility and dissolution properties

of the nanoparticles (Betriu et al., 2021;Amin et al., 2023; L. Zhang et al., 2019;Elkarim et al. , 2022).

Hydrogels are composed of polymers that can be crosslinked to form a network structure with a high water-absorbing capacity.(A. M. Mohammed et al., 2020a; Zheng et al., 2019). Thermosensitive hydrogels exhibit a transition from a gel to a sol state upon temperature changes. These hydrogels can contract upon injection, entrapping the loaded content and controlling its release. (Merisko-liversidge & Liversidge, 2008; Rani et al., 2022; Hassan et al., 2022; Elkarim & El-shenawy, 2022; A. M. Mohammed et al., 2020a; Du et al., 2021). Chitosan polymer is biocompatible and biodegradable, making it well-tolerated by the body and capable of gradual degradation, eliminating the need for additional removal surgeries(Zheng et al., 2019; Zheng et al., 2019; Du et al., 2021;Balo et al., 2010). Chitosan hydrogel provides protection to drugs against degradation and inactivation, especially in harsh physiological environments. The gel matrix acts as a barrier, shielding the drug from enzymatic degradation or pH-related instability, improving its stability and bioavailability (Balo et al., 2010; A. M. Mohammed et al., 2020b; Du et al., 2021).

Chitosan hydrogel can encapsulate drugs within its gel matrix, enabling controlled release pattern. The porous structure of the hydrogel allows for diffusion of drugs at a controlled rate, leading to sustained drug release over an extended period (Balo et al., 2010; A. M. Mohammed et al., 2020a; Du et al., 2021; Balo et al., 2010). Moreover, Chitosan hydrogel allows for localized drug delivery by direct application to the target site. This is particularly advantageous for treatment of localized diseases (Balo et al., 2010; Du et al., 2021;Dora et al., 2017).

Various formulations have been developed by researchers to enhance the solubility and bioavailability of Erlotinib. These include the utilization of complexing agents such as α-cyclodextrin, β-cyclodextrin, HP-β-cyclodextrin, and phospholipids (Tóth et al., 2016;Mandal et al., 2016; Dora et al., 2017; Uddin & Ju, 2020) . Additionally, nano preparations have been employed to improve the solubility of Erlotinib(Mandal et al., 2016; Fathi et al., 2017; Pandey et al., 2019; Moradpour & Barghi, 2019; L. Zhang et al., 2019; Pandey et al., 2019;). However, these approaches have certain limitations. Some of these limitations may be associated with factors like drug loading capacity, stability, or potential toxicity. For example, the use of chemical solvents or multiple stabilizers in these formulations may pose risks to human health. It is essential to consider these limitations and explore alternative strategies to address them while developing Erlotinib formulations with improved solubility and bioavailability.

The primary objective of this study was to enhance the solubility of Erlotinib (ETB) by developing stable Erlotinib Nanoparticles (ETB-NPs) without the use of excessive stabilizers and excipients. This was achieved by reducing particle size and increasing the surface area of the drug, leading to improved solubility and dissolution. Span-stabilized nanoparticles were prepared using the solvent anti-solvent technique, where dimethyl sulfoxide (DMSO)/Methyl alcohol (1:4 ratio) served as the solvent and water acted as the anti-solvent. The nanocrystals obtained were subjected to various characterizations, including particle size, solubility, in vitro dissolution, and dissolution kinetics. Additionally, the study focused on formulating ETB-NPs in chitosan hydrogel

to achieve a local, controlled, and targeted therapeutic effect. The chitosan hydrogel formulation was evaluated for organoleptic properties, viscosity, drug content, in vitro drug release, and dissolution kinetics.

Figure 1; illustrates the chemical structures of Erlotinib, Chitosan, Pluronic F127, and β-Glycerophosphate disodium salt.
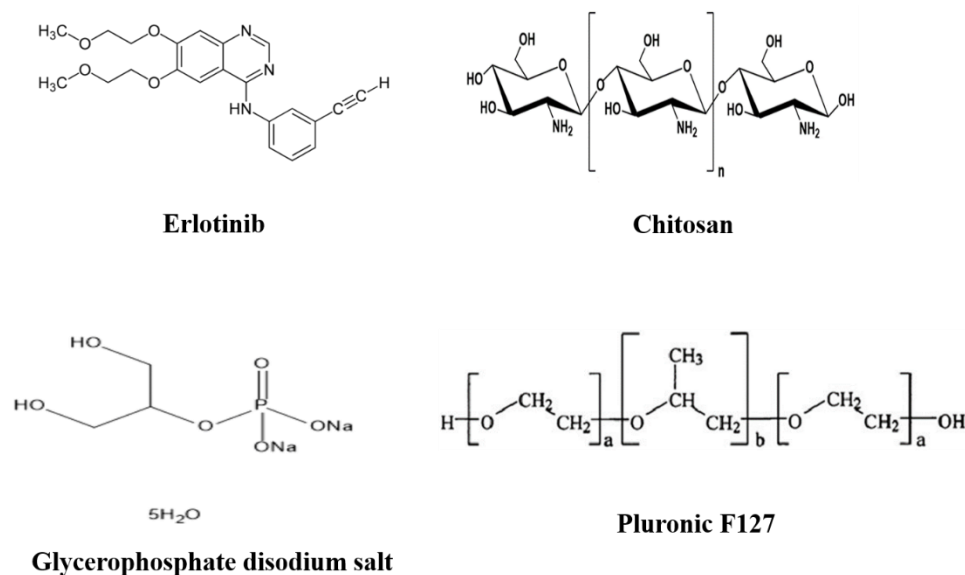

Figure 1. Chemical structure of Erlotinib (anticancer drug), Chitosan, β-Glycerophosphate disodium salt, and Pluronic F127.

2- Materials and Methods

2.1. Materials

Erlotinib (ETB) was purchased from Applichem for Pharmaceuticals Co., GmbH (Darmstadt, Germany). Chitosan (Mwt, 100–300 kDa and 95% acetylation degree) was provided by Biosyn-tech Inc. (Laval, QC, Canada). β-glycerophosphate pentahydrate (β-GP, Mwt 308 Da) were purchased from Loba Chemie PVT LTD. (Mumbai, India). Pluronic F127 (Mwt 12,800 Da) was obtained from Fluka Biochemika (Buchs, Switzerland). Methyl alcohol, DIMSO and all other materials and solvents were of analytical purity and used without further purification

2.2. Methods

2.2.1 Preparation of ETB-nanoparticles

Erlotinib nanoparticles (NPs) were prepared by solvent/anti-solvent precipitation technique. In this method, dimethylsulphoxide/methanol mixture (water miscible organic solvent) is considered as the solvent. While as, water was utilized as anti-

solvent. Span 80 was utilized as a surface stabilizer. The required amounts of ETB (10 mg) and span80 (5mg) were dissolved in 10 ml of solvent mixture (1:4, v/v ratio) of DIMSO/methanol in a test tube under sonication for 3 minutes at room temperature until a clear solution was obtained. The produced solution was then slowly added dropwise into 50 ml of distilled water by the aid of a syringe (over 20 minutes) under continuous stirring at room temperature using an overhead magnetic stirrer (Daihan Scientific Co., Korea) adjusted at 1000 rpm. To ensure evaporation of the organic solvents, the mixture was stirred for additional 2 hrs. To obtain pure NPs, the produced nano suspension was centrifuged, using high speed centrifuge (Mumbai, India), at 10000 rpm for 30 minutes. The supernatant was discarded, and the precipitated nanoparticles were washed twice with distilled water and dried under vacuum (Zeamil Horyzont Co., Poland) at 50° C for 24 h. The modified ETB-NPs were stored in a desiccator until further use (Mostafa et al., 2022; Gadhiya et al., 2021; Amin et al., 2023; Hassan et al., 2022).

2.2.2 Characterization of ETB-NPs

2.2.2.1. Size measurement

The size, size distribution, and polydispersion index (PDI) were measured at room temperature using Zetasizer (Malvern Zetasizer 300 HAS, Malvern Instruments, UK). Practically, 3 ml of an aqueous solution of each sample (prepared in PBS) was adjusted at 25 C and then allowed to expose to a laser beam of ≈633 nm at a scattering angle of ≈90°. The measurements were carried out in triplicate for each sample. The obtained results were presented as the average of the three measurements ±SD, whereas each measurement was run ≈20 times (with a≈10 s duration) (H. A. Mohammed et al., 2019; Shariare et al., 2018; Okafor and Aigbavboa, 2019).

2.2.2.2. Determination of Saturation Solubility

Generally, the saturation solubility of materials depends mainly on the temperature and the properties of the dissolution medium. However, below a size of approximately 1-2 μm, the saturation solubility is also a function of particle size(Pressure et al., 2015) . The saturation solubility of pure drug, physical mixture, and Span stabilized nanoparticles were determined in phosphate buffer (pH, 6.8). Typically, an excess amount of each sample was added to 10 ml of the buffer in screw glass tubes which were shacked at 50 rpm for 48 hrs in a thermostatically controlled water bath shaker fixed at 37 °C. Afterwards, samples were centrifuged at 10000 rpm at 4 °C and the drug concentration in supernatants was then analyzed spectrophotometrically (Shimadzu Co., Japan) at λmax 334 nm(Agrawal et al., 2004) .

2.2.2.3. Determination of the Production Efficiency (PE)

PE of the modified ETB-NPs was determined by dissolving a known amount (5 mg) of completely dried nanoparticles powder in methanol/DMSO and diluted with phosphate buffer (pH 7.4). The drug concentration was measured spectrophotometrically at 334 nm. The production efficiency of ETB nanocrystals was calculated using equation 1 (Mothilal et al., 2014).

PE % = Weight of ETB in NPs /Total weight of NPs $\times$ 100   eq (1)

2.2.4. In vitro Dissolution Studies

The in vitro dissolution profiles of either native ETB or ETB-NPs were performed using USP dissolution apparatus type II (Dissolution test apparatus, SR II, 6 flasks, paddle type, Hanson research Co., USA). Typically, 10 mg of either pure drug or an equivalent amount of the modified drug NPs was dispersed in 900 ml of PBS ((pH 7.4) which was stirred at 100 rpm and maintained at 37±1 °C for 2 hrs. At specified interval times, a liquate of 10 ml samples was taken, filtered using filter tip, and replaced immediately with an equal volume of fresh dissolution medium to maintain the dissolution volume constant. The drug concentration was determined spectrophotometrically (Shimadzu 1601, Japan) at λmax 334 nm. Each experiment was done three times and the results were presented graphically as the cumulative percent of dissolved drug against time.

2.2.5. Kinetic treatment of ETB-NPs dissolution data

The in vitro dissolution data were analyzed using various kinetic models, including zero order, first order, Higuchi diffusion, and Korsmeyer-Peppas models ((A. M. Mohammed et al., 2020b; Mostafa et al., 2022) as presented in **Tables 1 and 2**. The objective was to determine the most suitable dissolution model that accurately describes the drug dissolution pattern . The selection of the model was based on the coefficient of determination (R^2) values as recommended by Burnham and Anderson ((Y. Zhang et al., 2010) Amin, Osman, et al., 2023;Mostafa et al., 2022; Rani et al., 2022; Paarakh et al., 2018).

Table 1. Kinetic equations for different kinetic models (zero order, first order, Higushi diffusion and Korsmeyer-Peppas (A. M. Mohammed et al., 2020b)

Kinetic Model	Equations
Zero Order	$Q_t = Q_0 - K_0t$
First Order	$\text{Log } Q_t = \log Q_0 - K_1t/2.303$
Higushi's equations	$Q_t = Kh\sqrt{t}$
Korsmeyer-Peppas	$\log Q_t = \text{Log}K + n\text{Log}t$

Where Qt is the quantity of the drug dissolved at time t, K is the dissolution rate constant, and n is the diffusional exponent that characterizes the best fitted release mechanism (Y. Zhang et al., 2010).

Table 2. Parameters for characterizing drug curve (Y. Zhang et al., 2010)

Model	Equation
MRT	$MRT = \dfrac{\int_0 t \cdot (100-y) \cdot dt}{\int_0 (100-y) \cdot dt}$
MDT	$MDT = \dfrac{\sum_{1=1}^{n} -T_i \Delta M!}{\sum_{1=1}^{n} T \Delta M!}$
VDT	$VDT = \dfrac{\sum_{i=1}(t_i - MDT)}{\sum_{i=1}^{n} \Delta M_1}$
RD	$RD = \dfrac{VDT}{MD\Gamma^2}$
DE	$DE = \int_0 \dfrac{t \quad y \cdot dt}{y_{100} t} X 100\%$

Dissolution Efficiency (**DE**); Mean Dissolution Time (**MDT**) ; Mean Retention Time (**MRT**); Relative Dispersion (**RD**); and Variance of Dissolution Time (**VDT**).

2.2.6. Preparation of chitosan hydrogel loaded ETB-NPs

Different chitosan/Pluronic F127 hydrogel systems were constructed according to the previously reported method (Abdellatif et al., 2022; Berger et al., 2005). Practically, a 1.8% w/v chitosan solution was prepared using 0,1M acetic acid as solvent. To obtain a solution mixture of Pluronic/β-GP Also, 10% w/v pluronic solution and 35% w/v β-GP solution were prepared using distilled water. Then, the aqueous solution was added gradually to chitosan solution at 0 ◦C for 15 min until the hydrogel formation. For comparison, a separate hydrogel system was prepared according to the previous procedure but without the addition of Pluronic solution or without addition of β-GP solution. The composition of different hydrogel systems was presented in **Table 3**. The drug loading was achieved by incorporating unmodified ETB and ETB-NPs at a concentration of 1% w/v into the chitosan solution before crosslinking by gentle stirring until complete dissolution. Then, the prepared unmodified ETB and ETB-NPs loaded hydrogel systems were stored in the refrigerator at 8 ◦C until further experiments.

Table 3. Composition of different chitosan hydrogel systems loaded with ETB

Formulation code	Drug	Chitosan/acetic acid	Cross linking agent solutions	
			β-GP/water	Pluronic F127/water
F1	1%	1.8 %	35%	-
F2	1%	1.8%	-	10%
F3	1%	1.8%	35%	10%

2.2.7. Characterization of the prepared pure chitosan hydrogels

2.2.7.1. Drug content

A one-gram sample was prepared, containing either unmodified ETB or ETB-NPs equivalent to 1 mg of ETB. To dissolve the sample, an appropriate quantity of a mixture of dimethyl sulfoxide (DMSO) and ethyl alcohol was used. The resulting solution was then subjected to filtration using a Whatman filter paper to remove any impurities or solid particles.(Lee et al., 2021). The obtained filtrate was further diluted with distilled water to an appropriate concentration. The drug content was determined using a UV-Visible Spectrophotometer at 334 nm.

2.2.7.2. Visual Inspection (Organoleptic Properties)

The prepared systems underwent visual examination in both sol and gel forms to assess their purity, homogeneity, fluidity, and presence of phase separation.

2.2.7.3. pH Determination

The pH values of the prepared hydrogel systems were determined using an Ama Digital pH meter (Ama Co., Germany). The probe of the pH meter was immersed directly into the samples, enabling straightforward and accurate measurement of the pH values of the hydrogel systems.

2.2.7.4. Viscosity Measurement

An Ostwald U tube capillary viscometer was used to evaluate the viscosity of the produced chitosan hydrogel solutions at room temperature (25±1°C). In the viscometer, the liquid is briefly added till the level reaches the target. In order for the viscometer to reach the proper temperature, it is positioned vertically in a thermostatic bath. Once the liquid level is just over the mark, the sample volume is adjusted and the liquid is sucked or blown into the other arm. When the pressure or suction is removed, the time for the liquid to fall from the top mark to the bottom mark is recorded (H. A. Mohammed et al., 2019;LLOYD, 1958). Chitosan hydrogels' viscosity was assessed at 37°C using a Brookfield DV-III ultra-viscometer and a T-bar spindle (T-D 94) spinning at 50 rpm (Abdellatif et al., 2022).

2.2.7.5. Syringeability and injectability

The ability of dosage form to be easy injectable is very important issue. Noteworthy. the injectable system should have a suitable consistency in order to be released through the syringe needle into skin layers(Ramstack et al., 2002) **.** Therefore, the injectability test was carried out by filling a syringe with the hydrogel solution at room temperature and then allowed to be injected into a meat sample by the aid of finger pressure(Ramstack et al., 2002).

2.2.7.6. Sol-Gel Transition Temperature Measurement

To determine the gelation temperature (Tgel), the cold solutions of various hydrogel systems were heated on a water bath. The temperature range used for heating ranged from 8 to 40°C, and the heating process was conducted at a constant rate (1°C /min) with continuous stirring at a rate of shear (30 rpm). During the heating process, the gelation of the hydrogel systems was indicated by the point at which the magnetic bar within the solution stopped to move. At this point, the temperature was recorded as the gelation temperature (Tgel) for each respective hydrogel system (Balo et al., 2010).

2.2.8. In Vitro Drug Release Studies

Design of Experiment (DOE) was employed as a statistical technique to investigate and comprehend the influence of various factors, both individually and in combination, on the responses or outcomes of interest, with the aim of optimizing these responses and analyzing the factors under study. Examining each factor separately can be a laborious and time-consuming task. However, by utilizing a full factorial design, these limitations can be overcome as it allows for the simultaneous optimization of multiple factors, thereby reducing the total number of experiments required to achieve process optimization(Seyed Shahabadi & Reyhani, 2014;Arena et al., 2007;Amin, Amin, et al., 2023).

In the current study, the primary and interactive effects of two experimentally studied factors, namely "Drug " and "Chitosan Hydrogel Formula," were investigated using model equations designed by a three-level full factorial design. The predicted results obtained from the full factorial design model exhibited high values of R^2, and the significance value (P-value) indicating agreement with the experimental data and confirming the appropriateness of the full factorial design model(Mishra & Singh, 2010; Shokri, 2018). Moreover, to study the effects of the independent variables, namely "Drug " and "Chitosan Hydrogel Formula," on the response variable "% release" and determine the optimal formula, a three-level two-factor full factorial design was implemented using JMP® (version 16, SAS, USA). JMP® was utilized to statistically analyze the results and visualize the findings, enabling a comprehensive exploration of the data (Shokri, 2018; Amin et al., 2023; Rostami et al., 2019)

Practically, Eppendorf tubes containing 0.5 ml samples were prepared, consisting either 0.5 mg of un-modified ETB or ETB-NPs. These samples were then incubated at 37°C for 1 hour to facilitate gelation. After gel formation, the gels were exposed to 1 ml of phosphate buffer solution at pH 7.4, maintained at 37°C and shaken at 50 rpm.(Mccarthy et al., 2021;A. M. Mohammed et al., 2020a). At specific time intervals, 0.5 ml samples were withdrawn from the system, and an equivalent volume of fresh buffer solution was added to maintain sink conditions. To determine the amount of drug released, a newly developed UV-spectrophotometric method was employed for simultaneous analysis of ETB. Each measurement was performed in triplicate, and the obtained data were reported as means ± standard deviation (SD).(A. M. Mohammed et al., 2020a).

2.2.9. Kinetic treatment of ETB-NPs dissolution data

The in vitro dissolution data were analyzed using various kinetic models, including zero order, first order (Y. Zhang et al., 2010), Higuchi diffusion, and Korsmeyer-Peppas models (A. M. Mohammed et al., 2020b ; Mostafa et al., 2022). The objective was to determine the most suitable dissolution model that accurately describes the drug dissolution pattern. The selection of the model was based the coefficient of determination (R^2) values as recommended by Burnham and Anderson (Y. Zhang et al., 2010; Amin et al., 2023;Mostafa et al., 2022). **Table 1 and 2** represent the utilized kinetic equations.

3. Results and discussions

3.1. Preparation of ETB-NPs

Particle size, polydispersity index (PDI) and surface charge (zeta potential) are considered as the most important parameters for characterization the prepared nanocrystals. Particle size is considered as a reflective mirror for physicochemical properties such as physical stability, dissolution pattern, saturation solubility, and bioavailability. Also, pharmacokinetic parameters and therapeutic efficacy of the particular drug may be affected by the heterogeneity of size distribution (Janga et al., 2012). **Figure 2** showed the size and PDI of the modified ETB-NPs. the results indicated the successful formation of ETB nanoparticles via the anti-solvent method. The relatively uniform particle size and shape, with a low PDI of 0.13 and 100% intensity for ETB with an average size of 230 nm, indicates that the nanoparticles are relatively uniform in size and shape, which is desirable for pharmaceutical applications.
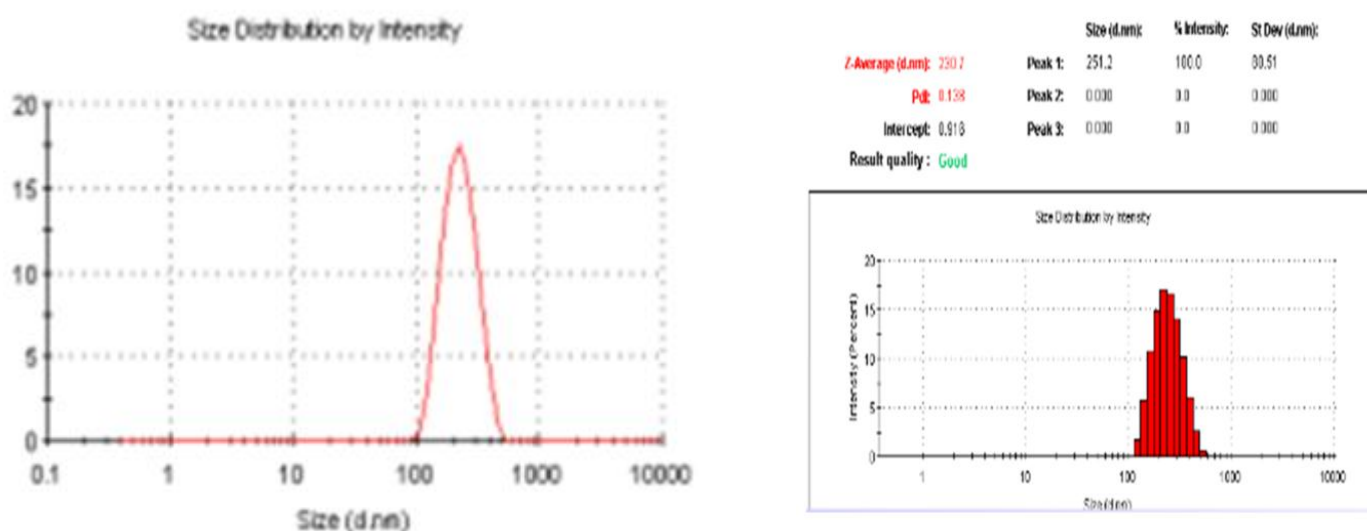

Figure 2. The size and size distribution of the modified ETB nanocrystal.

3.2.In vitro drug dissolution

Figure 3 display the in vitro dissolution profile of ETB and ETB-NPs. The results show that the formulated nanoparticle achieved a drug dissolution rate of approximately 100% in 105 minutes in either phosphate buffer(pH7.4) or distilled water. This represents a 7-fold increase in drug release compared to pure ETB, which only achieved a drug release of 14.4% in distilled water. In phosphate buffer (PH 7.4), ETB-NPs exhibited a 22-fold increase in drug release, with approximately 100 % drug dissolution within 105 minutes, compared to only 4.68% drug dissolution for pure ETB. The significant enhancement in dissolution can be attributed to the particle size reduction of ETB-NPs to the molecular level, which increases the surface area.

During a 60-minute period, ETB-NPs exhibited a 67% release rate, whereas pure ETB demonstrated only an 8.6% release rate in distilled water, resulting in an eight-fold increase in dissolution. In Phosphate buffer (pH7.4), ETB-NPs showed a 68% release rate, while pure ETB exhibited only a 17% release rate, resulting in a four-fold increase in dissolution.
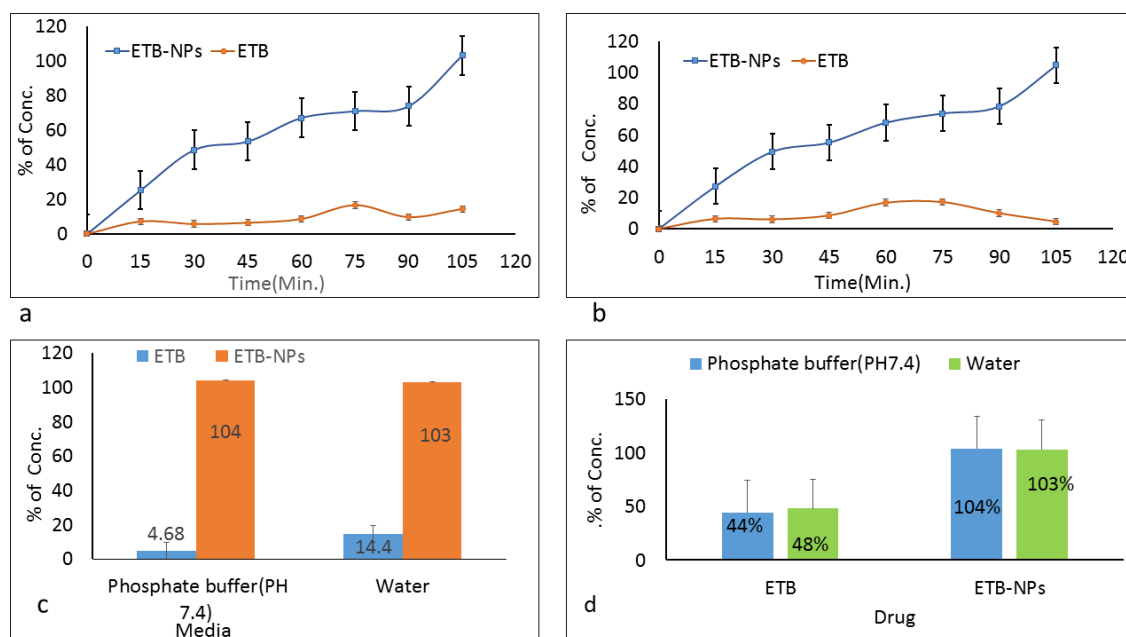

Figure 3. The dissolution profiles for ETB and ETB-NPS in distilled water (a); and in Phosphate buffer (PH. 7.4) (b); also, it represents bar plot for comparison between the effect of distilled water and phosphate buffer (PH. 7.4|) on the release data profiles of ETB and ETB-NPs (c), and bar plot comparison between the release data profiles of ETB and ETB-NPs in distilled water and phosphate buffer (d).

The significant enhancement of ETB solubility, achieved via NPs formation, may have important implication for their potential use as drug delivery systems. The high surface area to volume ratio of nanoparticles can increase the dissolution rate of poorly soluble drugs, resulting in faster onset of action and improved therapeutic efficacy(Shariare et al., 2018).

3.3. Kinetic treatment of dissolution data profile of ETB and ETB-NPs

The dissolution data of ETB were analyzed using four kinetic models: zero-order, first-order, Peppas and Higuchi models. The analysis was performed separately for two different dissolution media: distilled water and phosphate buffer (pH 7.4), the obtained results were tabulated in **(Tables 4 and 5).**

Whether in distilled water or phosphate buffer (pH7.4), the dissolution of ETB followed the zero order kinetic model, as indicated by the high values of determination coefficient R^2, which was obtained from the analysis **(Tables 4 and 5)**.

Table 4. kinetic data treatment for dissolution of ETB and ETB-NPs in different media

Kinetic Model		ETB-NPs		ETB	
		D. Water	Phos.Buffer	D.Water	Phos.Buffer
Zero Order	K_0	0.987	1.016	0.15	0.139
	R^2	0.9777	0.9264	0.6978	0.2067
First Order	K_1	0.019	0.02	0.002	0.002
	R^2	0.8637	0.891	0.6176	0.012
Higushi diffusion	k_H	8.612	8.87	1.317	1.288
	R^2	0.918	0.9408	0.5154	0.0621
Korsmeyer-Peppas	k_{KP}	4.962	5.217	1.156	4.436
	n	0.629	0.625	0.530	0.206
	R^2	0.9805	0.9705	0.5035	0.0727
Best fitted model		Kors. -Peppas		Zero order	Zero order

Regarding ETB-NPs, the dissolution mechanism, whether in distilled water or phosphate buffer (pH 7.4), was described by the Korsmeyer-Peppas model **Figure 5**. Furthermore, the Fickian constant 'n' was calculated using the Korsmeyer-Peppas model, which helps distinguish different release processes. In conclusion, the approach employed to enhance the solubility of ETB played a significant role in the dissolution mechanism, as evidenced by the results presented in **Table 4**

Table 5. Parameters for characterizing dissolution curve of ETB and ETB-NPs in different media

Parameter	ETB		ETB-NPs	
	Distilled Water	Phosphate Buffer (pH 7.4)	Distilled Water	Phosphate Buffer (pH 7.4)
DE	0.087	0.09694	0.558	0.577
MDT	40.875	112.5	48.113	47
MRT	51.353	51.59	35.867	34.572
RD	0.690	2.2181	0.561	0.570
VDT	1152.98	28073.07	1298.916	1259.75

Dissolution Efficiency **(DE)**; Mean Dissolution Time **(MDT)** ; Mean Retention Time **(MRT)**; Relative Dispersion **(RD)**; and Variance of Dissolution Time **(VDT)**.

When quantitatively evaluating drug dissolution characteristics and comparing dissolution profiles using model-dependent approaches, it is crucial to select an appropriate model for fitting the data. Various statistical criteria are commonly employed to assess the goodness of fit of a model in this context.

Coefficient of determination (R^2) measures the proportion of the data variation that can be explained by the model (Y. Zhang et al., 2010)., namely R^2, was widely utilized for the evaluation of drug dissolution kinetic models and the comparison of dissolution profiles in model-dependent approaches.

Table 4 presents an analysis of the dissolution behavior of ETB-NPs in distilled water and phosphate buffer (pH 7.4) using different kinetic models. The results indicate a strong fit of the Korsmeyer-Peppas model to the dissolution data, as evidenced by high R^2 values of 0.9805 in distilled water and 0.9705 in phosphate buffer. These findings confirm the successful evaluation of ETB-NPs dissolution behavior using the Korsmeyer-Peppas kinetic model. The improved solubility of ETB resulting from nanoparticle formation is likely responsible for the favorable results observed in the dissolution kinetics model.

The dissolution behavior of ETB was examined in both distilled water and phosphate buffer (pH 7.4) using various kinetic models. The results indicate that the zero-order kinetic model adequately describe the dissolution of ETB in both media. This conclusion is supported by the values of R^2. In distilled water, the R^2 value of 0.6978 suggests a reasonable fit to the zero-order kinetic model. In phosphate buffer (pH 7.4), the fit to the zero-order kinetic model is weaker, as indicated by the lower R^2 value of 0.2067. Overall, these results suggest that the zero-order kinetic model provide a reasonable description of the dissolution behavior of ETB in both distilled water and phosphate buffer (pH 7.4). It is worth noting that the fair fit observed may be attributed to the low aqueous solubility of ETB.

Table 5 displays the results for ETB-NPs in distilled water, with DE (dissolution efficiency) of 0.558, MDT (mean dissolution time) of 48.113, MRT (mean residence time) of 35.867, RD (relative dissolution) of 0.561, and VDT (variance of dissolution time) of 1298.916. Notably, DE show relatively high value, while (MDT) and (MRT) exhibit low values compared to the other parameters in the table. These findings can be attributed to the significant improvement in ETB solubility resulting from the formation of nanoparticles, as well as the favorable dissolution rate observed for ETB-NPs in distilled water

Furthermore, when considering the dissolution of ETB-NPs in phosphate buffer (pH 7.4), the value of (DE) was relatively high, measuring 0.577. On the other hand, the values of (MDT), (MRT), (RD), and (VDT) were comparatively low, with values of 47, 34.572, 0.570, and 1259.75, respectively. These positive outcomes can be attributed to the favorable solubility of ETB-NPs in phosphate buffer (pH 7.4).

In contrast, when considering the dissolution of ETB (unmodified) in either distilled water or phosphate buffer (pH 7.4), the following values were observed. In distilled water: (DE) of 0.087, (MDT) of 40.875, (MRT) of 51.353, (RD) of 0.690, and (VDT) of

1152.98. In phosphate buffer (pH 7.4): (DE) of 0.09694, (MDT) of 112.5, (MRT) of 51.59, (RD) of 2.218, and (VDT) of 28073.07.

Comparing these values with the corresponding values for ETB-NPs, it becomes apparent that the aqueous solubility of ETB is significantly poorer when dissolved in distilled water. This is evidenced by the low value of (DE), as well as the high values of (MDT), (MRT), and (RD). kinetic data of dissolution profile of ETB&ETBNPs was illustrated in figures (4&5).
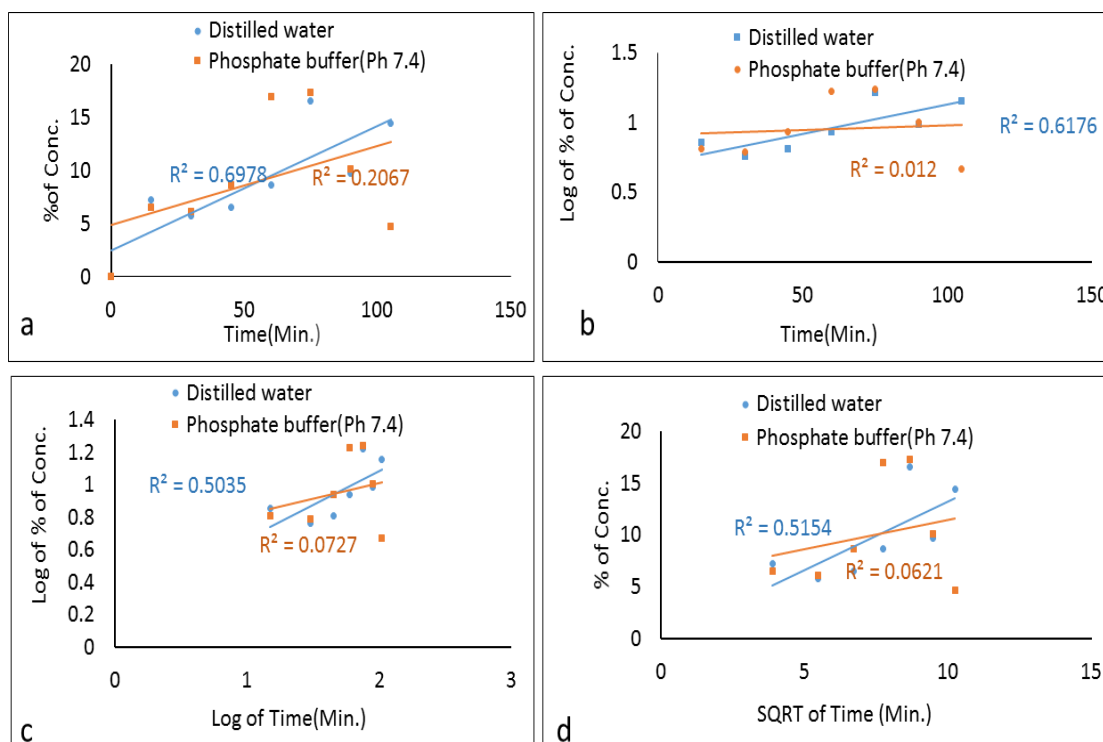

Figure 4. a Kinetic treatment of dissolution data profile of ETB in different media plotted according to zero order kinetic mechanism b: Kinetic treatment of dissolution data profile of ETB in different media plotted according to first order kinetic mechanism c: Kinetic treatment of dissolution data profile of ETB in different media plotted according Korsmeyer-Peppas mechanism d: Kinetic treatment of dissolution data profile of ETB in different media plotted according Higushi kinetic mechanism
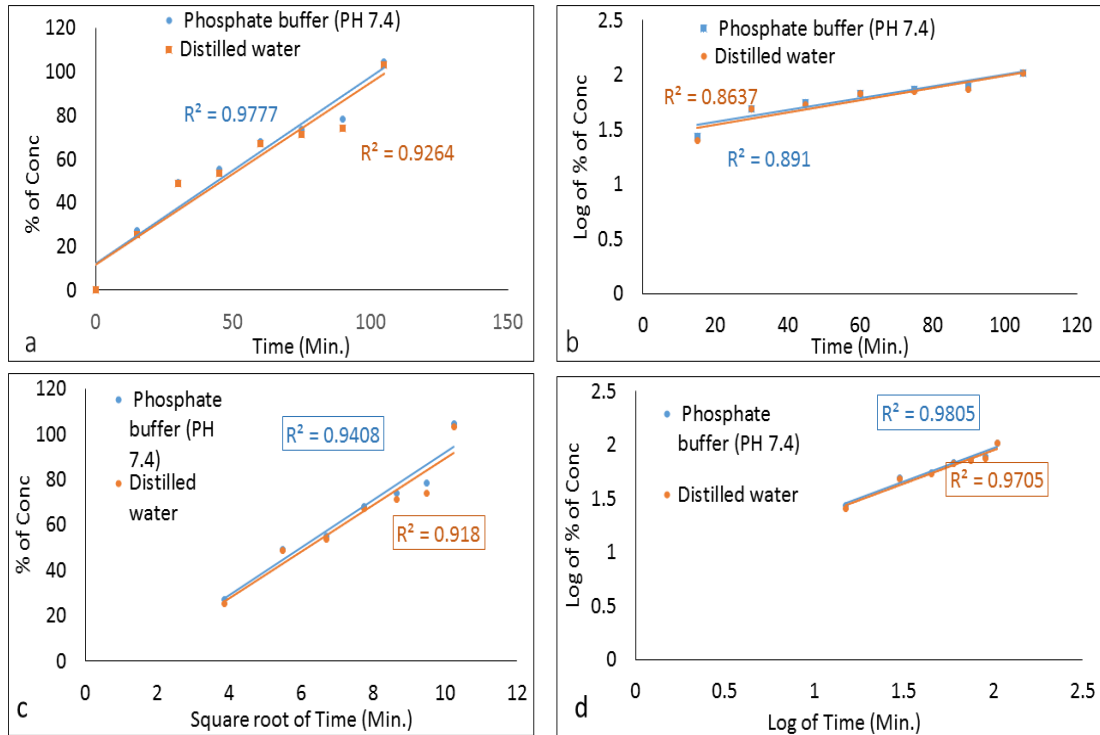
Figure 5. Kinetic treatment of dissolution data profile of ETB-NPs in different media plotted according to (a); zero order kinetic (b); first order kinetic (c); Higushi (d) Korsmeyer-Peppas kinetic mechanism.

3.4. Preparation of ETB-loaded Chitosan Hydrogels

The drug loading was achieved by incorporating unmodified ETB and ETB-NPs at concentration of 1% w/v into chitosan solution before crosslinking by stirring at 500rpm for 30 minutes to ensure uniform drug distribution.

3.5. Characterization of the prepared pure chitosan hydrogels
3.5.1.1.   Visual inspection (organoleptic properties)

Before and after the gelation process, the sensory qualities of the chitosan samples were assessed visually. The results showed that there were no lumps or signs of phase separation in either the liquid or gel states, and that all of the formulations had a uniform and homogeneous texture. The liquid was transparent and colourless, whereas the gel had a whitish, hazy appearance.

3.5.2.   pH determination

The produced chitosan hydrogels for PL F127 and β-GP were found to have a pH range of 6.9 to 7.3, as shown in the **Table 6**. This pH range shows that the injectable suitability of all the formulations. Injectable hydrogels should have a pH between 6.5-7.4 in order to prevent cell damage, according to earlier study (Gupta P et al. ,2002).

Table 6. The physicochemical properties (drug content, pH, viscosity, gelation point, and syringeability) of the modified chitosan hydrogel systems

Code	Drug content %	pH	Viscosity (cp*10³)		Gelation Point (°C)	Syringeability
			Sol(cp)	Gel(cp)		
F1	102±2.5	6.9 ± 1.0	110 ± 5.1	114 ± 8	35.4 ± 0.5	4.5.4 ± 0.5
F2	103± 4.75	7.1 ± 0.06	113.2 ± 2.7	117.8 ± 1.04	24.4 ± 1.1	5.4 ± 0.7
F3	103± 3.5	7.3 ± 0.06	148.3 ± 4.2	153 ± 4.58	29.2 ± 1.0	7.1 ± 0.8

3.5.3.   Viscosity measurements

The produced hydrogels' viscosity measurements in both the sol and gel stages are shown in **Table 6**. Because water is the main ingredient in all of the formulations, the results show that all hydrogel solutions have a comparable level of viscosity. For instance, the gel state viscosities for CH/ -GP, CH/PL F127, and CH/ -GP (35%)/ PL F127 (10%) were 114 Cp, 117.8, and 153 Cp, respectively. The increased interaction between the crosslinkers and the chitosan solution after mixing may be the cause of the higher viscosity in the gel state. On the other hand, the sol state viscosities for CH/ -GP (35%), CH/PL F127 (10%), and CH/ β-GP (35%/PL F127 (10%), respectively, were determined to be 110 Cp, 137.2 Cp, and 148.3. The CH/ β-GP (35%)/ PL F127 (10%) exhibited the maximum viscosity, measuring at 148.3.

3.5.4.   Syringeability and injectability

For injectable hydrogels to guarantee a specific level of syringeability and injectability, it is significant to note that the sol-gel transition phenomenon is a fundamental prerequisite. The cross-linking agents used were either 35% -GP, 10% PL F127, or 35% -GP-10% PL F127. With light to moderate finger pressure, these solutions may be smoothly and easily extruded from a 5 mm syringe, yielding a consistent 0.5 cm of solution in 5–10 seconds **(Table 6)**. These results indicate that these solutions are suitable for syringe injection testing with meat samples which comes with patient compliance.

3.5.5.   Sol-gel transition temperature measurement

All of the synthesized chitosan solutions underwent a sol-to-gel transition in response to temperature changes. The temperature at which gelation takes place for each formulation is displayed in **Table 6**. It is thought that the mechanisms underlying these sol-to-gel transitions involve a switch in the equilibrium from monomer to micelle, development of the micelle, or expansion of the micelle coupled with an increase in the

number of aggregations brought on by hydrophobic or attractive forces (Liu D-M et al.2001; Jeong B et al., 2012).

3.5.6. *In vitro* drug release studies

Design of experiments (DOE) facilitates the simultaneous assessment of the impact of drug and chitosan hydrogel formula as well as their actual significance on the % of drug release within seven days. **Table 7** describes the full factorial design. Investigation of the effect of drug and chitosan hydrogel formula revealed the significant effect of drug on % of drug release within seven days (P-value=0.00008) **(Figure 6)**, while chitosan hydrogel formula had statistically insignificant effect on % of release (P-value=0.57) (**Figure 7**). The interactive effect of drug and chitosan hydrogel formula was insignificant (P-value= 0.98), the experimental data had a high degree of correlation with the predicted response, the % of release actual Vs. the predicted plot had an R^2 of 1 and a P-value of 0.0002, The statistical factorial approach optimized the response using the desirability function. The desirability is a mathematical method used to spot the optimized formulation. The optimization was set for drug (ETB-NPs).

From factorial design we have selected ETB-NPs as drug dosage form exhibited the maximum % of release, Regarding ETB-NPs, there were notable variations in the percentage of drug release within one week among different formulas. Specifically, formula no. 2 exhibited a substantial release of 91.26%, whereas formula no. 1 resulted in a 30% release rate. Interestingly, formula no. 3, which is the reverse of the previous statement, showed a release percentage of 27.76%. In contrast, when considering ETB by itself, the release percentages from different formulas showed distinct patterns. Formula no. 2 had a significantly lower release rate of 2.65%, while formula no. 1 yielded a moderately higher release of 1.75%. Lastly, formula no. 3 had the lowest release percentage for ETB at 0.17%.

Table 7. Full factorial design run matrix and the obtained responses: drug and Chitosan hydrogel formula are the studied factors, while the %Release is the response

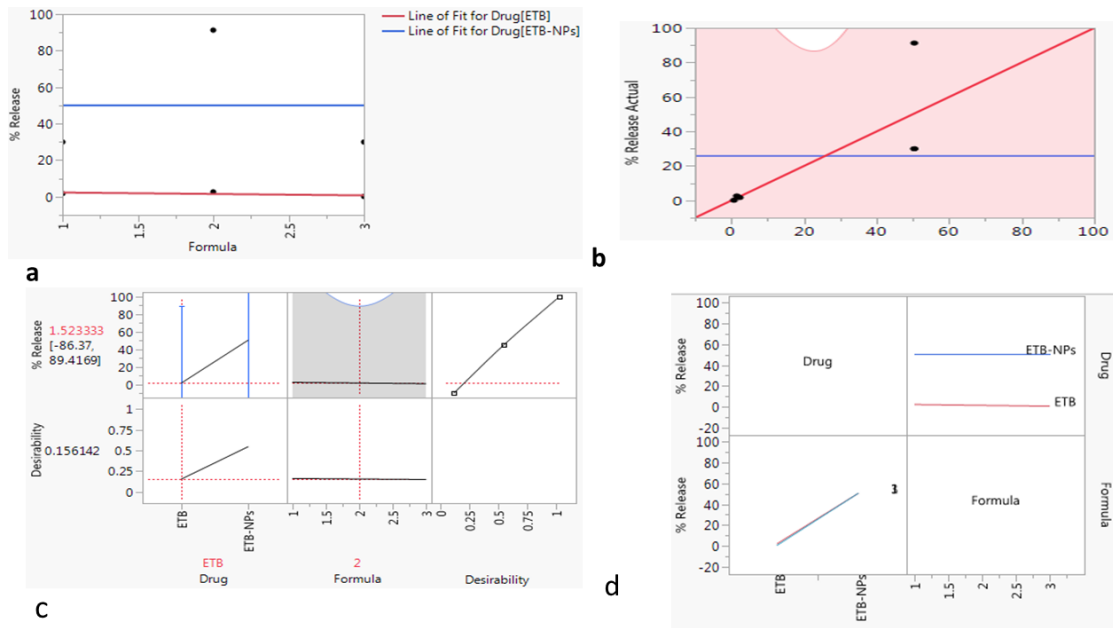| Full Factorial Design			
Number	**Independent Variables**		**Dependent Variable (% of drug release within seven days)**
	Drug	**Chitosan Hydrogel Formula**	
1	ETB	(F1)	1.75
2		(F2)	2.65
3		(F3)	0.17
4	ETB-NPs	(F1)	30
5		(F2)	91.26
6		(F3)	27.76

Figure 6. a:Regression plot b:Actual by predict plot c: Prediction profiler d: Interaction plot
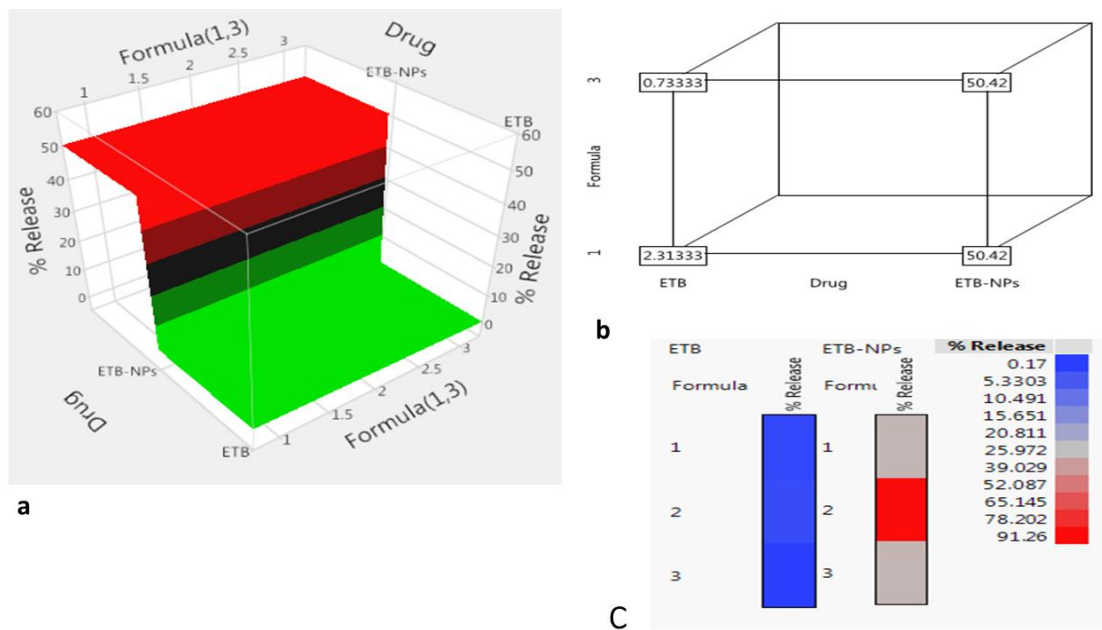

Figure 7. a: Surface plot b: Cube plot c: Cell plot

Figure 8 illustrates the effect of different chitosan hydrogel systems on the release profile of ETB and ETB-NPs. The results showed that the percentage of drug release was the highest from chitosan-pluronic F127 (104% drug release was achieved within 10 days for ETB-NPs but only 4.5% drug release was obtained within 30 days for native ETB), this attributed to the great enhancement of solubility of ETB by nanoparticle formation. On the other hand, the percentage of drug release were the smallest from chitosan/B-Glycerophosphate/Pluronic F127 (F3). Furthermore, the controlled release of drugs from nanoparticles can also prolong the duration of action and reduce the frequency of dosing, which can enhance patient compliance and reduce the potential for side effects.
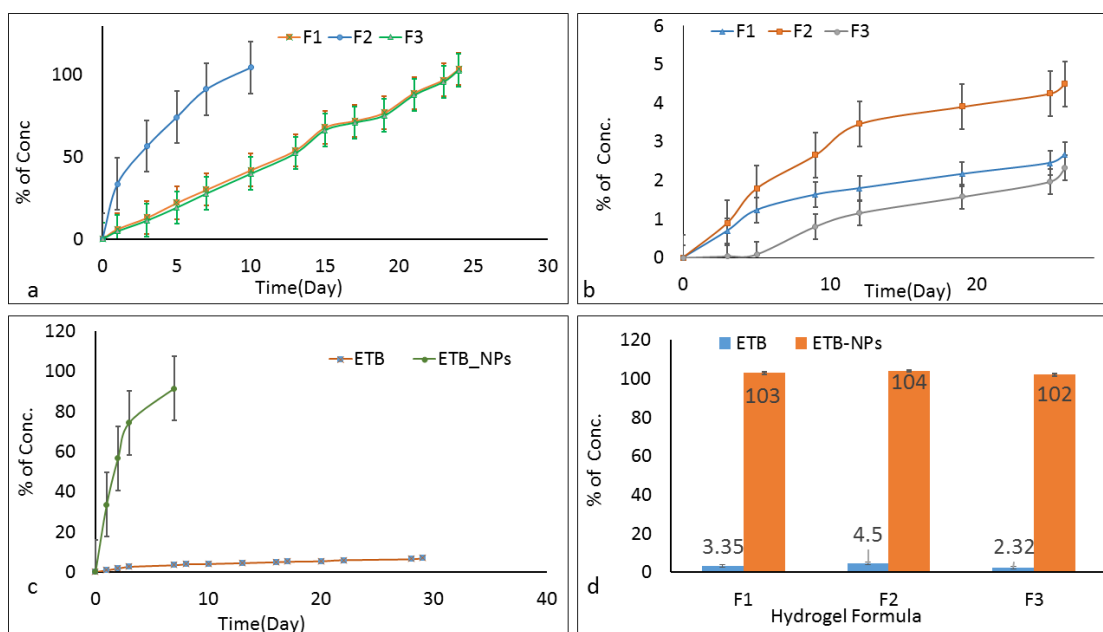

Figure 8. a: ETB-NPS release data profile from different hydrogel systems b: ETB release data profile from different hydrogel systems c: ETB and ETB-NPs release data profile from (F2) hydrogel system d: bar plot for comparison of release data profile of ETB and ETB-NPs from different chitosan hydrogel systems.

3.5.7. Kinetic analysis

The release data of ETB were analyzed using four kinetic models: zero-order, first-order, Peppas, and Higuchi models. The analysis was performed separately for three different chitosan hydrogel formula F1, F2 and F3 (**Figures 9 and 10 as well as Table 8 and 9**).

The release of ETB from chitosan hydrogel formula (F1) followed the Korsmeyer-Peppas mechanism, Higuchi model in case of F2 and Korsmeyer-Peppas mechanism in case of F3, as indicated by the high value of coefficient of determination (R^2) obtained from the analysis (**Figure 9).**
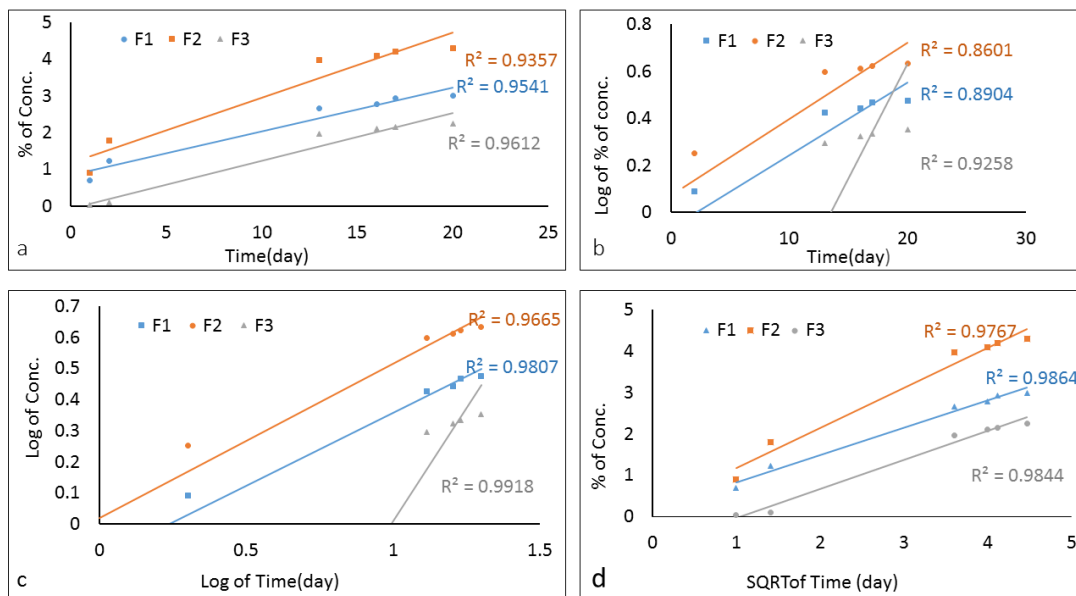
Figure 9. Kinetic treatment of release data profile of ETB from different chitosan hydrogel systems plotted according to zero order (**a**), first order (**b**), Korsmeyer-Peppas (**c**), and Higushi kinetic mechanism (**d**).

In case of ETB-NPs release from F1 followed to Kerseymere-Peppas mechanism, followed Higushi in case of F2 while from F3 it was followed zero order kinetic mechanism (**Figure 10**).
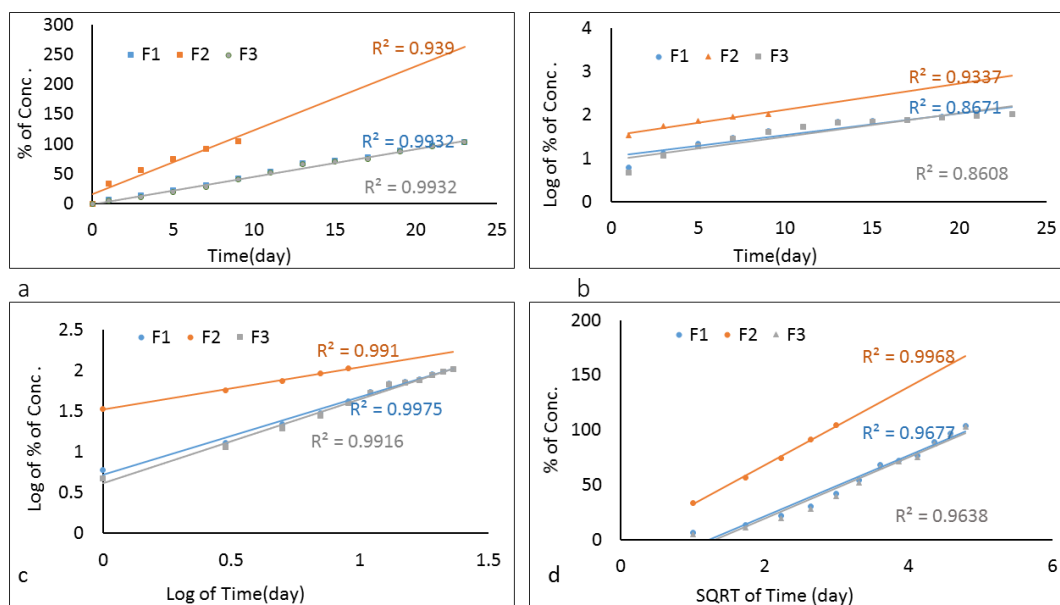

Figure 10: Kinetic treatment of release data profile of ETB-NPs from different chitosan hydrogel systems plotted according to zero order (**a**), first order (**b**), Korsmeyer-Peppas (**c**), and Higushi kinetic mechanism (**d**).

Table 8: kinetic treatment for ETB and ETB-NPs release data profile from different chitosan hydrogel systems

Kinetic Model		ETB			ETB-NPs		
		F1	F2	F3	F1	F2	F3
Zero Order	K_o	0.187	0.285	0.128	4.663	13.054	4.571
	R^2	0.9541	0.9357	0.9612	0.9932	0.939	0.9932
First Order	K^1	0.002	0.003	0.001	0.082	0.319	0.079
	R^2	0.8904	0.8601	0.9258	0.8671	0.9337	0.8608
Higushi diffusion	k_H	0.722	1.113	0.467	18.3	34.101	17.866
	R^2	0.9864	0.9767	0.9844	0.9677	0.9968	0.9638
Korsmeyer-Peppas	k_{KP}	0.901	1.594	0.154	5.2	31.901	4.424
	N	0.411	0.356	0.933	0.961	0.537	1.011
	R^2	0.9807	0.9665	0.9918	0.9975	0.991	0.9916
Best fitted model		Higushi	Higushi	Kors.-Peppas		Higushi	Zero Order

Table 8 presents an analysis of the release behavior of ETB and ETB-NPs from different chitosan hydrogel systems using various kinetic models. For ETB-NPs in formula F1, the results indicate a strong fit of the Korsmeyer-Peppas model to the release, as evidenced by high R^2 value of 0.997. These finding confirm the successful evaluation of ETB-NPs release behavior using the Korsmeyer-Peppas kinetic model. Regarding the release mechanism of ETB-NPs from formula F2, it was observed that the release mechanism follows Higushi diffusion model, as indicated from the values of R^2 value of 0.9968 (Table 8). However, in the case of ETB-NPs release from hydrogel F3, the values of R^2 indicate a good fit of the zero-order kinetic model to the release, with value of 0.9932.

On the other hand, the release behavior of unmodified ETB from different gel formula was investigated. The results indicated that Higushi diffusion model adequately describes the release in formula F1, with R^2 value of 0.9864. Similarly, in formula F2, the Higushi diffusion model is also suitable for describing the release of ETB, with R^2 value of 0.9767. But, in the case of F3, the release of drug follows the Korsmeyer-Peppas model, as indicated from the highest value of R^2 (0.9918).

Table 9 displays the parameters for characterizing release data profile of ETB and ETB-NPs from different chitosan hydrogel systems. An analysis was conducted to examine the release behavior of ETB-NPs from various chitosan hydrogel systems using different kinetic models. The results obtained were as follows: For **F1:** The DE and MDT were **0.54, and 11**, respectively.

Table 9. parameters for characterizing release data profile of ETB and ETB-NPs from different chitosan hydrogel systems

Parameter	ETB			ETB-NPs		
	F1	F2	F3	F1	F2	F3
DE	0.022	0.034	0.013	0.54	0.666	0.39
MDT	5.40	4.032	8.439	11.00	3.27	8.26
MRT	9.96	9.947	9.95	6.98	2.32	6.51
RD	0.92	1.11	0.23	0.33	0.65	0.26
VDT	27.00	18.12	16.61	40.50	6.96	18.31

Dissolution Efficiency (**DE**); Mean Dissolution Time (**MDT**)؛ Mean Retention Time (**MRT**); Relative Dispersion (**RD**); and Variance of Dissolution Time (**VDT**).

Regarding gel **F2**, the values of DE, and MDT, were **0.666, 3.27,** respectively. Whiles as in the case of **F3**, the values were **0.39, and 8.26**, respectively. From the obtained results it could be concluded that the release from F2 demonstrated the highest DE and the smallest MDT, VDT, and MRT, compared with the other two investigated gel formula. The obtained results come in a good agreement with results of in vitro release studies. These findings can be attributed to the significant improvement in ETB solubility resulting from the formation of nanoparticles. Additionally, the favorable dissolution rate observed for ETB-NPs in distilled water contributes to these results.

Regarding the release of unmodified ETB from different chitosan hydrogel systems, the following values were obtained: In the case F1, the dissolution efficiency DE was **0.022**, mean dissolution time (MDT) was **5.4**, the relative dissolution (RD) was **0.92**. whiles as in the case of F2, the results showed that the values of DE, MDT, and RD were **0.034**, **4.032**, and **1.11**, respectively. Also, the obtained values in the case of F3 were **0.013**, **8.439**, **and 0.23**, respectively. As a conclusion, among these systems, F2 exhibited the highest dissolution efficiency and relative dissolution and the lowest MDT compared with either F1 and F3.

By taking F2 as a selected formula in order to compare between the modified and the unmodified Drug, the results which was presented in table 8 showed that the obtained very low DE value **(0.034)** of pure drug from F2 compared with that of ETB-NPs **(0.666)** can be attributed to the poor aqueous solubility of ETB. Also, the limited solubility of ETB may hinder its dissolution and subsequent release from the chitosan hydrogel systems, leading to lower DE values compared to ETB-NPs, which increased the drug surface area and consequently improved solubility due to nanoparticle formation.

4. Conclusion

To enhance the solubility of ETB, we employed a highly effective strategy involving the formation of nanoparticles. Simultaneously, we aimed to address the systemic side effects of ETB by implementing a localized delivery method using an injectable hydrogel. Chitosan hydrogel emerged as the ideal platform for precisely delivering ETB, accommodating both unmodified ETB and ETB-NPs. Our research

findings underscored that the most substantial drug release was achieved through the nanoparticle formation process, outperforming the release rate of traditional ETB delivery. Notably, these modified nanoparticles had an average size of approximately 230 nm. In conclusion, these results emphasize the promising potential of ETB in cancer treatment, offering enhanced safety and a reduction in undesirable side effects

REFERENCES

Abdellatif, A. A. H., Mohammed, A. M., Saleem, I., Alsharidah, M., Al Rugaie, O., Ahmed, F., & Osman, S. K. (2022). Smart Injectable Chitosan Hydrogels Loaded with 5-Fluorouracil for the Treatment of Breast Cancer. *Pharmaceutics*, *14*(3). https://doi.org/10.3390/pharmaceutics14030661

Agrawal, S., Pancholi, S. S., Jain, N. K., & Agrawal, G. P. (2004). Hydrotropic solubilization of nimesulide for parenteral administration. *International Journal of Pharmaceutics*, *274*(1–2), 149–155. https://doi.org/10.1016/j.ijpharm.2004.01.012

Amin, H., Amin, M. A., Osman, S. K., & Mohammed, A. M. (2023). Chitosan nanoparticles as a smart nanocarrier for gefitinib for tackling lung cancer : Design of experiment and in vitro cytotoxicity study International Journal of Biological Macromolecules Chitosan nanoparticles as a smart nanocarrier for gefitinib for . *International Journal of Biological Macromolecules*, *246*(June), 125638. https://doi.org/10.1016/j.ijbiomac.2023.125638

Amin, H., Osman, S. K., Mohammed, A. M., & Zayed, G. (2023). Gefitinib-loaded starch nanoparticles for battling lung cancer: Optimization by full factorial design and in vitro cytotoxicity evaluation. *Saudi Pharmaceutical Journal*, *31*(1), 29–54. https://doi.org/10.1016/j.jsps.2022.11.004

Arena, R., Myers, J., Williams, M. A., Gulati, M., Kligfield, P., Balady, G. J., Collins, E., & Fletcher, G. (2007). Assessment of functional capacity in clinical and research settings: A scientific statement from the American Heart Association committee on exercise, rehabilitation, and prevention of the council on clinical cardiology and the council on cardiovascular n. *Circulation*, *116*(3), 329–343. https://doi.org/10.1161/CIRCULATIONAHA.106.184461

Balo, E., Karavana, S. Y., Hyusein, I. Y., & Köse, T. (2010). *Design and Formulation of Mebeverine HCl Semisolid Formulations for Intraorally Administration*. *11*(1). https://doi.org/10.1208/s12249-009-9374-3

Berger, J., Reist, M., Chenite, A., Felt-baeyens, O., Mayer, J. M., & Gurny, R. (2005). *Pseudo-thermosetting chitosan hydrogels for biomedical application*. *288*, 17–25. https://doi.org/10.1016/j.ijpharm.2004.07.036

Betriu, N., Andreeva, A., & Semino, C. E. (2021). Erlotinib promotes ligand-induced EGFR degradation in 3D but not 2D cultures of pancreatic ductal adenocarcinoma cells. *Cancers*, *13*(18), 1–20.

https://doi.org/10.3390/cancers13184504

Dora, C. P., Kushwah, V., Katiyar, S. S., Kumar, P., Pillay, V., Suresh, S., & Jain, S. (2017). Improved oral bioavailability and therapeutic efficacy of erlotinib through molecular complexation with phospholipid. *International Journal of Pharmaceutics*, *534*(1–2), 1–13. https://doi.org/10.1016/j.ijpharm.2017.09.071

Du, W., Zong, Q., Guo, R., Ling, G., & Zhang, P. (2021). *Injectable Nanocomposite Hydrogels for Cancer Therapy*. *2100186*, 1–21. https://doi.org/10.1002/mabi.202100186

Elkarim, R. A. A., & El-shenawy, A. A. (2022). *vitro / in vivo evaluation Novel nanosized Diacerein proliposomes for oral delivery : Development and in vitro / in vivo evaluation*. *July*. https://doi.org/10.7324/JAPS.2022.120714

Erdoğar, N., Akkın, S., Varan, G., & Bilensoy, E. (2021). Erlotinib complexation with randomly methylated β-cyclodextrin improves drug solubility, intestinal permeability, and therapeutic efficacy in non-small cell lung cancer. *Pharmaceutical Development and Technology*, *26*(7), 797–806. https://doi.org/10.1080/10837450.2021.1946695

Gadhiya, D. T., Patel, J. K., & Bagada, A. A. (2021). An impact of nanocrystals on dissolution rate of Lercanidipine: Supersaturation and crystallization by addition of solvent to antisolvent. *Future Journal of Pharmaceutical Sciences*, *7*(1). https://doi.org/10.1186/s43094-021-00271-x

Hassan, N. A., Darwesh, O. M., Smuda, S. S., Altemimi, A. B., Hu, A., Cacciola, F., Haoujar, I., & Abedelmaksoud, T. G. (2022). *Recent Trends in the Preparation of Nano-Starch Particles*. *1 4*, 1–24.

Honeywell, R. J., Kathmann, I., Giovannetti, E., Tibaldi, C., Smit, E. F., Rovithi, M. N., Verheul, H. M. W., & Peters, G. J. (2020). Epithelial transfer of the tyrosine kinase inhibitors erlotinib, gefitinib, afatinib, crizotinib, sorafenib, sunitinib, and dasatinib: Implications for clinical resistance. *Cancers*, *12*(11), 1–18. https://doi.org/10.3390/cancers12113322

Lee, S. Y., Yang, M., Seo, J. H., Jeong, D. I., Hwang, C., Kim, H. J., Lee, J., Lee, K., Park, J., & Cho, H. J. (2021). Serially pH-Modulated Hydrogels Based on Boronate Ester and Polydopamine Linkages for Local Cancer Therapy. *ACS Applied Materials and Interfaces*, *13*(2), 2189–2203. https://doi.org/10.1021/acsami.0c16199

LLOYD, H. E. (1958). A simple capillary viscometer. *Journal of Clinical Pathology*, *11*(4), 363–365. https://doi.org/10.1136/jcp.11.4.363

Mandal, B., Mittal, N. K., Balabathula, P., Thoma, L. A., & Wood, G. C. (2016). Development and in vitro evaluation of core-shell type lipid-polymer hybrid nanoparticles for the delivery of erlotinib in non-small cell lung cancer. In

European Journal of Pharmaceutical Sciences (Vol. 81). Elsevier B.V. https://doi.org/10.1016/j.ejps.2015.10.021

Mccarthy, P. C., Zhang, Y., & Abebe, F. (2021). *Recent Applications of Dual-Stimuli Responsive Chitosan Hydrogel Nanocomposites as Drug Delivery Tools*.

Merisko-liversidge, E. M., & Liversidge, G. G. (2008). *Toxicologic Pathology Drug Nanoparticles : Formulating Poorly*. https://doi.org/10.1177/0192623307310946

Mishra, A. K., & Singh, V. P. (2010). A review of drought concepts. *Journal of Hydrology*, *391*(1–2), 202–216. https://doi.org/10.1016/j.jhydrol.2010.07.012

Mohammed, A. M., Osman, S. K., Saleh, K. I., & Samy, A. M. (2020a). In Vitro Release of 5-Fluorouracil and Methotrexate from Different Thermosensitive Chitosan Hydrogel Systems. *AAPS PharmSciTech*, *21*(4), 1–11. https://doi.org/10.1208/s12249-020-01672-6

Mohammed, A. M., Osman, S. K., Saleh, K. I., & Samy, A. M. (2020b). *In Vitro Release of 5-Fluorouracil and Methotrexate from Different Thermosensitive Chitosan Hydrogel Systems*. 1–11. https://doi.org/10.1208/s12249-020-01672-6

Mohammed, H. A., Al-omar, M. S., El-readi, M. Z., Alhowail, A. H., Aldubayan, M. A., & Abdellatif, A. A. H. (2019). *Formulation of Ethyl Cellulose Microparticles Incorporated Pheophytin A Isolated from Suaeda vermiculata for Antioxidant and Cytotoxic Activities*. 1–12.

Moradpour, Z., & Barghi, L. (2019). Novel approaches for efficient delivery of tyrosine kinase inhibitors. *Journal of Pharmacy and Pharmaceutical Sciences*, *22*, 37–48. https://doi.org/10.18433/jpps29891

Mostafa, H. M., Osman, S. K., & Zayed, G. (2022). *NANOCRYSTALLIZATION OF DAPSONE ; A NOVEL APPROACH TO BOOST SOLUBILITY , DISSOLUTION , AND IN- VITRO ANTI-INFLAMMATORY ACTIVITY*. *66*, 1–28.

Mothilal, M., Krishna, M. C., Teja, S. P. S., Manimaran, V., & Damodharan, N. (2014). *Formulation and evaluation of naproxen-eudragit ® RS 100 nanosuspension using 32 factorial design FORMULATION AND EVALUATION OF NAPROXEN-EUDRAGIT ® RS 100 NANOSUSPENSION USING 3 2 FACTORIAL DESIGN*. *February 2017*.

Paarakh, M. P., Jose, P. A. N. I., Setty, C. M., & Peter, G. V. (2018). *RELEASE KINETICS – CONCEPTS AND APPLICATIONS*. 12–20.

Pandey, P., Chellappan, D. K., Tambuwala, M. M., Bakshi, H. A., Dua, K., & Dureja, H. (2019). Central composite designed formulation, characterization and in vitro cytotoxic effect of erlotinib loaded chitosan nanoparticulate system. *International Journal of Biological Macromolecules*, *141*, 596–610. https://doi.org/10.1016/j.ijbiomac.2019.09.023

Pressure, H., Technique, H., J, A. K., Ramkanth, S., S, L. P., & Gopal, V. (2015). *Enhancement of Saturation Solubility and In Vitro Dissolution of Carvedilol Enhancement of Saturation Solubility and In Vitro Dissolution of Carvedilol Nanoparticles by High Pressure Homogenization Technique. December.*

Ramstack, I. J. M., Us, M. A., Hotz, J. M., & Riley, M. G. I. (2002). *(12) United States Patent. 1*(12).

Rani, K. R. V., Rajan, S., Bhupathyraaj, M., Priya, R. K., Halligudi, N., Al-ghazali, M. A., Sridhar, S. B., Shareef, J., Thomas, S., Desai, S. M., & Pol, P. D. (2022). *The Effect of Polymers on Drug Release Kinetics in Nanoemulsion In Situ Gel Formulation.* 1–13.

Rostami, M., Mazaheri, H., Hassani Joshaghani, A., & Shokri, A. (2019). Using Experimental Design to Optimize the Photo-degradation of P-Nitro Toluene by Nano-TiO2 in Synthetic Wastewater. *International Journal of Engineering, Transactions B: Applications*, *32*(8), 1074–1081. https://doi.org/10.5829/ije.2019.32.08b.03

Salehi, N., Kuminek, G., Al-gousous, J., Sperry, D. C., Greenwood, D. E., Waltz, N. M., Amidon, G. L., Zi, R. M., & Amidon, G. E. (2021). *Improving Dissolution Behavior and Oral Absorption of Drugs with pH-Dependent Solubility Using pH Modi fi ers : A Physiologically Realistic Mass Transport Analysis.* https://doi.org/10.1021/acs.molpharmaceut.1c00262

Seyed Shahabadi, S. M., & Reyhani, A. (2014). Optimization of operating conditions in ultrafiltration process for produced water treatment via the full factorial design methodology. *Separation and Purification Technology*, *132*, 50–61. https://doi.org/10.1016/j.seppur.2014.04.051

Shariare, M. H., Sharmin, S., Jahan, I., Reza, H. M., & Mohsin, K. (2018). The impact of process parameters on carrier free paracetamol nanosuspension prepared using different stabilizers by antisolvent precipitation method. *Journal of Drug Delivery Science and Technology*, *43*(October 2017), 122–128. https://doi.org/10.1016/j.jddst.2017.10.001

Shokri, A. (2018). Application of Sono–photo-Fenton process for degradation of phenol derivatives in petrochemical wastewater using full factorial design of experiment. *International Journal of Industrial Chemistry*, *9*(4), 295–303. https://doi.org/10.1007/s40090-018-0159-y

Tóth, G., Jánoska, Á., Szabó, Z. I., Völgyi, G., Orgován, G., Szente, L., & Noszál, B. (2016). Physicochemical characterisation and cyclodextrin complexation of erlotinib. *Supramolecular Chemistry*, *28*(7–8), 656–664. https://doi.org/10.1080/10610278.2015.1117083

Uddin, M. S., Ju, J. &Yang e (2020). *Journal of Polymer Research*, *27*(3).

Wang, W., Hao, X., Chen, S., Yang, Z., Wang, C., Yan, R., Zhang, X., Liu, H., Shao, Q., & Guo, Z. (2018). SC. *Polymer.* https://doi.org/10.1016/j.polymer.2018.10.067

Zhang, L., Wang, J., Zhang, Y., Ke, L., Lin, X., Li, Z., Chen, H., & Gao, Y. (2019). Indocyanine green-encapsulated erlotinib modified chitosan nanoparticles for targeted chemo-photodynamic therapy of lung cancer cells. *Dyes and Pigments,* *170*(May), 107588. https://doi.org/10.1016/j.dyepig.2019.107588

Zhang, Y., Huo, M., Zhou, J., Zou, A., Li, W., Yao, C., & Xie, S. (2010). *DDSolver : An Add-In Program for Modeling and Comparison of Drug Dissolution Profiles.* *12*(3). https://doi.org/10.1208/s12248-010-9185-1

Zheng, Y., Wang, W., Zhao, J., Wu, C., & Ye, C. (2019). Preparation of injectable temperature-sensitive chitosan-based hydrogel for combined hyperthermia and chemotherapy of colon cancer. *Carbohydrate Polymers, 222*(January), 115039. https://doi.org/10.1016/j.carbpol.2019.115039

صياغة وتوصيف هيدروجيل الشيتوزان الحساس للحرارة و المحمّل بعقار الايرلوتينيب: التصميم الشامل لبيانات الإطلاق

عرفات عبد الظاهر¹ أحمد محمد محمد² شعبان خلف عثمان²*

¹ الهيئة العامة للتأمين الصحي ، فرع جنوب الصعيد ، مصر.

² قسم الصيدلانيات والتكنولوجيا الصيدلانية ، كلية الصيدلة ، جامعة الأزهر ، أسيوط ٧١٥٢٤ ، مصر

البريد الالكتروني للباحث الرئيسي: shaabanosman@azhar.edu.eg

يعد عقار ال (ايرلوتينيب) اجد مثبطات انزيم التيروزين كاينيزز .وهو يستخدم بفاعلية في علاج أنواع مختلفة من الأورام التي تعبر عن بروتين EGFR. وهو دواء ضعيف الذوبان في الماء وله ارتباط شديد لبروتينات بلازما الدم .وفقًا لنظام تصنيف المستحضرات الصيدلانية الحيوية (BCS) ، يندرج عقار الايرلوتينيب Erlotinib تحت الفئة الثانية ، حيث تعمل قابليته للذوبان كخطوة جوهرية لتحديد معدل التوافر البيولوجي .في الإعطاء الجهازي ، يُظهر Erlotinib توافرًا حيويًا بنسبة ٧٥ ٪ تقريبًا ، ولكنه يسبب أيضًا العديد من الآثار الجانبية ، والتي يمكن أن تكون شديدة في بعض الحالات بسبب ضعف قابليتها للذوبان في الماء وارتباطها القوي ببروتينات البلازما .لمعالجة مشكلة التوافر البيولوجي المنخفض ، اتبعنا نهجًا فعالًا لتعزيز قابلية ذوبان Erlotinib. تم استخدام تكوين الجسيمات النانوية باستخدام طريقة استعمال السوائل المرسبة ، و قد تمت دراسة خواص الجزيئات النانومترية المحضرة بأكثر من طريقة منها قياس حجم وتوزيع الجزيئات باستخدام تقنية التشتت الضوئي الحركي . كما تم دراسة الذوبان في المختبر لتوصيف الجسيمات النانوية Erlotinib (ETB-NPs). أنتجت هذه الدراسات أيضًا نتائج إيجابية ، مما يدل على التحسين الناجح لقابلية ذوبان Erlotinib من خلال تكوين الجسيمات النانوية . بعد تعزيز الذوبان ، بالاضافة الي ذلك فقد تمت صياغة الدواء في صورة هلام مائي حساس للحرارة و قابل للحقن مباشرة داخل الجسم حيث يكون في صورة سائل قابل للحقن بواسطة السرنجة ثم يتكون تلقائيا داخل الورم الموجود بالجسم عند درجة حرارة الجسم . أظهرت هذه الصيغة تحسينات كبيرة في إطلاق Erlotinib. أدى تحسين قابلية الذوبان والتحكم الموضعيي لـ Erlotinib داخل البيئة الدقيقة للورم إلى تسهيل التحكم في انطلاق العقار وساهم في التحسينات الملحوظة .وقد تم توصيف هيدروجيل الشيتوزان المستخدم كنظام ناقل لـ Erlotinib بدقة باستخدام تقنيات مختلفة ، بما في ذلك قياسات اللزوجة وتحديد الاس الهيدروجيني ودراسات الإنطلاق في المختبر ، وكلها أسفرت عن نتائج إيجابية.

الكلمات المفتاحية: إرلوتينيب ، السرطان ، التيروزين كيناز ، الهلاميات المائية ، الانطلاق الدوائي في المختبر ، الجسيمات النانوية ، الشيتوزان